Gazi Üniversitesi
**Fen Bilimleri Dergisi**
PART C: TASARIM VE TEKNOLOJİ

Gazi University
**Journal of Science**
PART C: DESIGN AND TECHNOLOGY

GU J Sci, Part C, 13(3): 1184-1194 (2025)

# Effects of in-situ formed $TiB_2$ Phase on Mechanical Properties of Spark Plasma Sintered Boron Carbide

Sinem BAŞKUT[1*], Name YALAMA[1], Servet TURAN[1]

[1]*Eskisehir Technical University, Faculty of Engineering, Department of Materials Science and Engineering, Eskisehir, Türkiye*

***Article Info***

*Research article*
*Received: 14/05/2025*
*Revision: 29/06/2025*
*Accepted: 30/06/2025*

***Keywords***

*$B_4C$*
*$TiB_2$*
*Fracture Toughness*
*Hardness*
SPS

***Makale Bilgisi***

*Araştırma makalesi*
*Başvuru: 14/05/2025*
*Düzeltme: 29/06/2025*
*Kabul: 30/06/2025*

***Anahtar Kelimeler***

*$B_4C$*
*$TiB_2$*
*Kırılma Tokluğu*
*Sertlik*
*SPS*

***Graphical/Tabular Abstract (Grafik Özet)***

*This study investigated the effects of $TiO_2$ additions on $B_4C$ sintered via SPS. The in-situ formed $TiB_2$ phase contributed to the improvement of fracture toughness of $B_4C$ through various toughening mechanisms. / Bu çalışma, SPS yöntemiyle sinterlenmiş $B_4C$'ye $TiO_2$ ilavelerinin etkilerini araştırmıştır. In-situ olarak oluşmuş $TiB_2$ fazı, çeşitli tokluk mekanizmaları yoluyla $B_4C$'nin kırılma tokluğunun artmasına katkıda bulunmuştur.*

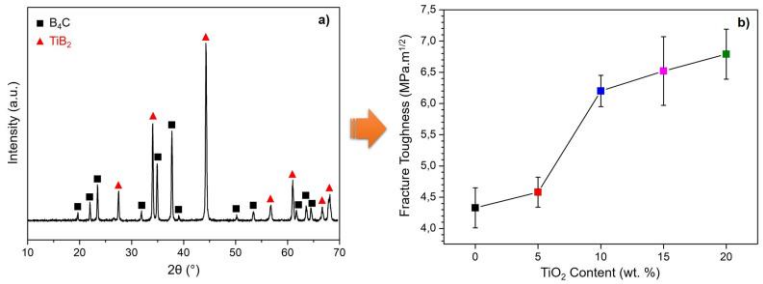


**Figure A**: (a) XRD patern of the $B_4C$ containing 20 wt. % $TiO_2$ and (b) fracture toughness values of the $B_4C$s containing 5, 10, 15 and 20 wt. % $TiO_2$ / **Şekil A:** Ağırlıkça % 20 $TiO_2$ içeren $B_4C$'nin XRD paterni (b) Ağırlıkça % 5, 10, 15 ve 20 $TiO_2$ içeren $B_4C$'lerin kırılma tokluk değerleri.

***Highlights (Önemli noktalar)***

- *In-situ $TiB_2$ phase was formed as a result of the reactions between $B_4C$ and $TiO_2$ during SPS. / SPS sırasında $B_4C$ ve $TiO_2$ arasında gerçekleşen reaksiyonlar sonucu in-situ $TiB_2$ fazı oluşmuştur.*
- *The toughening mechanisms provided by $TiB_2$ contributed to the improvement of fracture toughness of $B_4C$. / $TiB_2$'nin sağladığı tokluk mekanizmaları $B_4C$'nin kırılma tokluğunun iyileşmesine katkıda bulunmuştur.*
- *The relative density and hardness of $B_4C$ decreased with increasing $TiO_2$ content. / $TiO_2$ içeriği arttıkça $B_4C$'nin bağıl yoğunluğu ve sertliği azalmıştır.*

***Aim (Amaç):*** *Identify the second phases that may form during SPS when $TiO_2$ is used as a sintering additive in $B_4C$ matrix, and to evaluate their effects on the density and mechanical properties of the resulting composites. / $TiO_2$, $B_4C$ matrisinde sinterleme katkı maddesi olarak kullanıldığında, SPS işlemi sırasında oluşabilecek ikinci fazları belirlemek ve bu fazların elde edilen kompozitlerin yoğunluğu ve mekanik özellikleri üzerindeki etkilerini değerlendirmektir.*

***Originality (Özgünlük):*** *The fracture toughness of $B_4C$ was enhanced through the in-situ formation of $TiB_2$ using a cost-effective approach. / $B_4C$'nin kırılma tokluğu, ekonomik bir yöntemle in-situ $TiB_2$ oluşumu vasıtasıyla artırılmıştır.*

***Results (Bulgular):*** *The results revealed that an in-situ $TiB_2$ phase was formed as a result of the reactions between $B_4C$ and $TiO_2$ during SPS. The relative density and hardness of the $B_4C$ matrix slightly decreased with increasing $TiO_2$ content. The fracture toughness of the $B_4C$ matrix was enhanced by the presence of residual stress-induced microcracks and by toughening mechanisms such as crack deflection, bridging, and blocking promoted by the in-situ formed $TiB_2$ phase. / Sonuçlar, SPS sırasında $B_4C$ ile $TiO_2$ arasındaki reaksiyonlar sonucunda in-situ $TiB_2$ fazının oluştuğunu ortaya koymuştur. Artan $TiO_2$ içeriğiyle birlikte $B_4C$ matrisinin bağıl yoğunluğu ve sertliğinde hafif bir azalma gözlemlenmiştir. $B_4C$ matrisinin kırılma tokluğu, artık gerilme kaynaklı mikroçatlakların varlığı ve in-situ olarak oluşan $TiB_2$ fazı ile desteklenen çatlak saptırma, köprüleme ve durdurma gibi toklaştırma mekanizmaları sayesinde artırılmıştır.*

***Conclusion (Sonuç):*** *The fracture toughness of $B_4C$ was significantly improved through various toughening mechanisms provided by the in-situ formed $TiB_2$ phase throughout the matrix. / $B_4C$'nin kırılma tokluğu, in-situ olarak oluşmuş $TiB_2$ fazının matris boyunca sağladığı çeşitli tokluk mekanizmalarının yardımıyla önemli ölçüde iyileştirilmiştir.*

*Corresponding author, e-mail: skayhan@eskisehir.edu.tr
DOI: 10.29109/gujsc.1699270

GU J Sci, Part C, 13(3): 1184-1194 (2025)

Gazi Üniversitesi
**Fen Bilimleri Dergisi**
PART C: TASARIM VE TEKNOLOJİ

Gazi University
**Journal of Science**
PART C: DESIGN AND TECHNOLOGY

http://dergipark.gov.tr/gujsc

# Effects of in-situ formed $TiB_2$ Phase on Mechanical Properties of Spark Plasma Sintered Boron Carbide

Sinem BAŞKUT[1*], Name YALAMA[1], Servet TURAN[1]

*Eskisehir Technical University, Faculty of Engineering, Department of Materials Science and Engineering, Eskisehir, Türkiye*

***Article Info***

*Research article*
*Received: 14/05/2025*
*Revision: 29/06/2025*
*Accepted: 30/06/2025*

***Keywords***

*$B_4C$*
*$TiB_2$*
*Fracture Toughness*
*Hardness*
*SPS*

**Abstract**

Due to their superior properties, $B_4C$ ceramics are extensively utilized in applications such as defense and ballistic protection, coatings, aerospace, and high-temperature electronic devices. However, enhancing its low fracture toughness and poor sinterability would significantly expand its potential applications. In this study, the effects of $TiO_2$ as a sintering additive on the density and mechanical properties of $B_4C$ were investigated, along with the identification of in-situ second phases likely to form during sintering with SPS. To achieve this, $TiO_2$ was added to $B_4C$ in amounts of 5, 10, 15, and 20 wt. %. XRD analyses of the SPS-sintered samples confirmed the formation of an in-situ $TiB_2$ phase, resulting from reactions between $B_4C$ and $TiO_2$ during sintering. The release of CO gas from the reactions between $TiO_2$ and $B_4C$ during sintering led to a slight decrease in the relative density of the $B_4C$ matrix with increasing $TiO_2$ content. The results from density measurements were in agreement with BSE-SEM images. The addition of $TiO_2$ caused a minor decrease in the hardness of the $B_4C$ matrix. The fracture toughness of the $B_4C$ matrix improved by approximately 6, 43, 51, and 57 % with the addition of 5, 10, 15, and 20 wt. % $TiO_2$, respectively. This improvement has been attributed to the contribution of toughening mechanisms such as crack deflection, bridging, and blocking provided by the in-situ formed $TiB_2$, as well as the presence of stress-induced microcracks.

# In-situ Olarak Oluşmuş $TiB_2$ Fazının Spark Plazma Sinterleme ile Üretilmiş Bor Karbürün Mekanik Özellikleri Üzerine Etkileri

***Makale Bilgisi***

*Araştırma makalesi*
*Başvuru: 14/05/2025*
*Düzeltme: 29/06/2025*
*Kabul: 30/06/2025*

***Anahtar Kelimeler***

*$B_4C$*
*$TiB_2$*
*Kırılma Tokluğu*
*Sertlik*
*SPS*

**Öz**

$B_4C$ seramikleri üstün özellikleri nedeniyle savunma ve balistik koruma, kaplamalar, havacılık ve yüksek sıcaklıkta çalışan elektronik cihazlar gibi uygulamalarda yaygın olarak kullanılmaktadır. Ancak, düşük kırılma tokluğu ve zayıf sinterlenebilirliğinin iyileştirilmesi, bu malzemenin potansiyel kullanım alanlarını önemli ölçüde genişletecektir. Bu çalışmada, $TiO_2$'nin sinterleme ilavesi olarak $B_4C$'nin yoğunluğu ve mekanik özellikleri üzerindeki etkileri ile SPS yöntemiyle sinterleme sırasında oluşması muhtemel in-situ ikinci fazların belirlenmesi üzerinde durulmuştur. Bu amaçla, $TiO_2$ $B_4C$'ye ağırlıkça % 5, 10, 15 ve 20 oranlarında ilave edilmiştir. SPS ile sinterlenmiş numunelerin XRD analizleri, sinterleme sırasında $B_4C$ ile $TiO_2$ arasında gerçekleşen reaksiyonlar sonucunda in-situ $TiB_2$ fazının oluştuğunu göstermiştir. Sinterleme sürecinde $TiO_2$ ile $B_4C$ arasındaki reaksiyonlar sırasında açığa çıkan CO gazı nedeniyle, artan $TiO_2$ içeriğiyle birlikte $B_4C$ matrisinin bağıl yoğunluğunda az miktarda azalma gözlemlenmiştir. Yoğunluk ölçüm sonuçları, BSE-SEM görüntüleri ile uyumlu bulunmuştur. $TiO_2$ ilavesi, $B_4C$ matrisinin sertliğinde hafifçe azalmaya neden olmuştur. $B_4C$ matrisinin kırılma tokluğu, sırasıyla % 5, 10, 15 ve 20 $TiO_2$ katkısıyla yaklaşık % 6, 43, 51 ve 57 oranlarında artış göstermiştir. Bu iyileşme, in-situ olarak oluşmuş $TiB_2$'nin sağladığı çatlak saptırma, köprüleme ve durdurma gibi toklaştırma mekanizmalarının katkıları ile artık gerilme kaynaklı mikroçatlakların varlığıyla ilişkilendirilmiştir.

## 1. INTRODUCTION (GİRİŞ)

Boron carbide ($B_4C$) ceramics are widely used in various industrial applications due to their outstanding properties, including low density (2.52 g/cm³), excellent chemical inertness, high hardness (~3770 kg/mm²), high melting point (2427 °C), an elastic modulus of 450 GPa, and superior wear resistance. Common applications include body armor, cutting tools, mechanical seals, blast nozzles, wire-drawing dies, and neutron-absorbing components [1–5]. Despite these advantages, $B_4C$

*Corresponding author, e-mail: skayhan@eskisehir.edu.tr
DOI: 10.29109/gujsc.1699270

suffers from several limitations. It is difficult to densification owing to its low self-diffusion coefficient, often resulting in a porous microstructure. Additionally, its relatively low flexural strength and poor fracture toughness restrict its broader use as a structural engineering ceramic [6–8].

Sintering methods such as spark plasma sintering (SPS), hot pressing (HP), hot isostatic pressing (HIP), and pressureless sintering (PS) are commonly used to achieve high temperatures necessary for the densification of $B_4C$ [9]. Among these, PS is often preferred due to its cost-effectiveness. However, in the PS technique, excessive grain growth at elevated temperatures can adversely affect the densification of $B_4C$. To address this issue, the addition of sintering additives is a widely used approach. These additives help lower the sintering temperature and enhance both densification and the mechanical properties of $B_4C$. They can be carbon-based, metallic, oxide, non-oxide or a combination of these types [10]. In one study [11], the addition of 10 wt. % graphene platelets (GPLs) to the $B_4C$ matrix improved its fracture toughness by approximately 50 %. In another study [12], the incorporation of aluminum (Al) as a sintering additive significantly enhanced the density, fracture toughness, and strength of $B_4C$. Similarly, Kelvin et al. [13] reported that adding 5 wt. % $Al_2O_3$ to the $B_4C$ matrix led to nearly full densification (97 %) and a ~ 45 % increase in fracture toughness.

A review of the literature indicated that in-situ secondary phases can form due to reactions between added sintering additives and $B_4C$ during sintering [14-20]. These in-situ phases have been reported to enhance the fracture toughness of $B_4C$ by impeding crack propagation. For instance, in a study [15] where $ZrO_2$ was added to $B_4C$ and the SPS technique was used as the sintering method, it was determined that the fracture toughness increased from 2.3 $MPa.m^{1/2}$ to 3.96 $MPa.m^{1/2}$ due to the crack deflection and branching toughening mechanisms provided by the in-situ formed $TiB_2$ phase. Perevislov et al. [16] produced $B_4C$ matrix composites containing varying amounts of Si using HP, and reported that the fracture toughness of $B_4C$ increased by approximately 12 % due to the in-situ formation of a SiC phase. Liu et al. [17] examined $B_4C$ composites containing 5 wt. % metallic Ti sintered via PS and reported the in-situ formation of a $TiB_2$ phase, which increased the relative density from ~79 % to ~96 % and doubled the fracture toughness, attributed to crack-bridging, deflection, and branching mechanisms induced by the $TiB_2$ phase. Şahin et al. [18], who added 20 vol. % metallic Ti to the $B_4C$ matrix and identified the in-situ formation of $TiB_2$ after SPS sintering, achieved a fracture toughness value of 5.9 $MPa.m^{1/2}$. In a study [19] where titanium silicide ($Ti_5Si_3$) powder was added to the $B_4C$ matrix as a sintering additive, the in-situ formation of $TiB_2$ and SiC phases was observed during SPS sintering, and a significant improvement in the wear resistance of the $B_4C$ matrix was reported. In another study [20], where amorphous B, Ti, and graphite were added to $B_4C$ and the powder mixtures were sintered using SPS, $B_4C/TiB_2$ composites with varying ratios were obtained depending on the amounts of the starting powders, and fracture toughness values as high as $9.9 \pm 0.01$ $MPa.m^{1/2}$ were obtained.

Given these findings, the objective of the present study is to identify the second phase that may form during sintering with SPS when $TiO_2$ is used as a sintering additive in $B_4C$, and to evaluate its effects on the density and mechanical properties of the resulting composites. To this end, $TiO_2$ and $B_4C$ powders were mixed by ball milling and sintered using the SPS technique. The phases present in the sintered samples were identified via x-ray diffraction (XRD), while microstructures were examined using scanning electron microscopy (SEM). In addition, measurements of density, hardness, and fracture toughness were conducted during the study.

## 2. MATERIALS AND METHODS (MATERYAL VE METOD)

Commercially available $B_4C$ powder (CRS Chemicals, F2000 Grade, $d_{50}$ =1.61 µm) and $TiO_2$ (Acros Organics, 99 % Anatase, $d_{50}$ =5 µm) powder were used as starting materials. Prior to mixing, the $TiO_2$ powder was ball milled (Fritsch Pulverisette) at 300 rpm for 1 h in an isopropanol medium. $TiO_2$ was then added to the $B_4C$ powder at weight fractions of 5, 10, 15, and 20 %. Subsequently, $B_4C$ and $TiO_2$ powders were blended in a silicon nitride ($Si_3N_4$) jar with $Si_3N_4$ balls for 75 min. at 300 rpm in an isopropanol medium. After milling, isopropanol was removed using an evaporator, and the dried mixtures were sieved.

The prepared compositions were sintered using the SPS technique (HP 25D, FCT GmbH) at 1950 °C under a uniaxial pressure of 50 MPa for a dwell time of 20 min. in a vacuum atmosphere. The heating rate was set to 100 °C/min. The resulting sintered samples had a diameter of 20 mm and a thickness of 6 mm.

Bulk densities of the samples were measured using Archimedes' principle, with deionized water as the immersion medium. Relative density values were calculated based on the rule of mixtures. For the calculations, theoretical densities of $B_4C$ and $TiB_2$ were taken as 2.52 g/cm³ and 4.52 g/cm³, respectively.

XRD (Rigaku, RINT-2000) analyses were carried out to bulk samples between 10–70° (2Θ) under the conditions of 40 kV accelerating voltage, 15 mA current, 1 °/min. scan speed and 0.02 step size. Samples were sectioned and polished using an automatic polisher (STRUERS TegraPol-25), progressing from coarse to fine polishing steps. The polished surfaces of the samples were investigated by backscatter electron imaging (BSE-SEM) and energy dispersive spectroscopy (EDS-SEM, Oxford Instruments, INCA Energy) techniques in the SEM (Zeiss, SUPRA 50 VP).

Hardness measurements were conducted using the Vickers indentation method (Emco-Test) under a 5 kg load and a dwell time of 10 seconds. A minimum of ten indentations was made per sample, and the average values were used for statistical analysis. Fracture toughness was calculated using Equation 1 [21].

$$K_c = 0.067 \left(\frac{E}{H_V}\right)^{0.4} H_V \alpha^{0.5} \left(\frac{c}{a}\right)^{-1.5} \quad (1)$$

## 3. RESULTS AND DISCUSSION (SONUÇLAR VE YORUMLAR)

XRD spectra of the $B_4C$ matrix and $B_4Cs$ containing 5, 10, 15, and 20 wt.% $TiO_2$ are presented in Figure 1. XRD analysis of the pure $B_4C$ matrix revealed only the $B_4C$ phase, whereas the patterns of the $TiO_2$-containing $B_4Cs$ indicated the presence of both $B_4C$ and $TiB_2$ phases. This confirms that the in-situ $TiB_2$ phase was formed as a result of the reactions between $B_4C$ and $TiO_2$ during the sintering process, as described by Equation 2 [22, 23].

$$4B_4C(s) + 5\ TiO_2 \rightarrow 5TiB_2(s) + 4CO(g) + 6BO(g) \quad (2)$$

Furthermore, the absence of detectable $TiO_2$ peaks in the XRD spectra of the $TiO_2$-added $B_4Cs$ indicated that all the $TiO_2$ was consumed during the reactions. With increasing $TiO_2$ content, the intensity of the $TiB_2$ peaks increased, whereas the intensity of the $B_4C$ peaks gradually decreased. This trend suggested that a higher amount of $B_4C$ was consumed and more $TiB_2$ was formed with increasing $TiO_2$ content, consistent with previous findings [24].

BSE-SEM images of the $TiO_2$-containing $B_4C$ composites (Fig. 2 b1–e2) revealed two distinct phases, distinguished by white and gray contrasts. To identify the phases present, EDS-SEM analyses were performed on the polished surface of the $B_4C$ composite containing 10 wt.% $TiO_2$, as shown in Figure 3. For each phase, measurements were taken at five different points, and the average atomic percentages (atm. %) were then calculated. In the gray-contrast regions (Fig. 3b1 and 3b2), labeled as region 1 (green) in the BSE-SEM image (Fig. 3a), the atm. % of boron (B) and carbon (C) were approximately 80 % and 20 %, respectively (Fig. 3b1, b2). In contrast, the white-contrast regions labeled as Region 2 (orange) in Fig. 3a exhibited atm. % of boron (B) and titanium (Ti) of approximately 65 % and 35 %, respectively (Fig. 3c1, c2). Based on the EDS-SEM results, the gray contrast can be attributed to the $B_4C$ phase, while the white contrast corresponds to the $TiB_2$ phase. Considering the combined results from XRD, SEM imaging, and EDS-SEM analyses, the $TiO_2$-added $B_4C$ systems can be classified as in-situ formed $B_4C$–$TiB_2$ composites.

The BSE-SEM images of the $B_4C$–$TiB_2$ composites (Fig. 2, b1–e2) revealed that the in-situ formed $TiB_2$ phase is homogeneously distributed within the $B_4C$ matrix microstructure. Additionally, as observed in the images ranging from Fig. 2 b1 to e2, the in-situ formation of $TiB_2$ predominantly occurs along the $B_4C$ grain boundaries. Among the in-situ formed $B_4C$–$TiB_2$ composites, no significant porosity was observed in the microstructure of the sample containing 5 wt. % $TiO_2$ (Fig. 2 b1 and b2). In contrast, noticeable porosities are evident in the samples containing 10, 15, and 20 wt. % $TiO_2$ (Fig. c1–e2). Some of these porosities may result from grain pull-out during mechanical polishing. However, the majority of the porosity is likely due to the release of CO gas generated by the in-situ reaction during the sintering process [9].

Table 1 presents the bulk and relative density values of the $B_4C$ matrix and in-situ $B_4C$–$TiB_2$ composites. The $B_4C$ matrix exhibited a bulk density of 2.49 g/cm³ and a relative density of 98.8 %, indicating that the material was nearly fully densified. These density measurements align well with the microstructural observations of $B_4C$ matrix shown in Fig. 2 a1 and a2, which reveal no significant porosity. The addition of $TiO_2$ resulted in an increase in bulk density but a decrease in relative

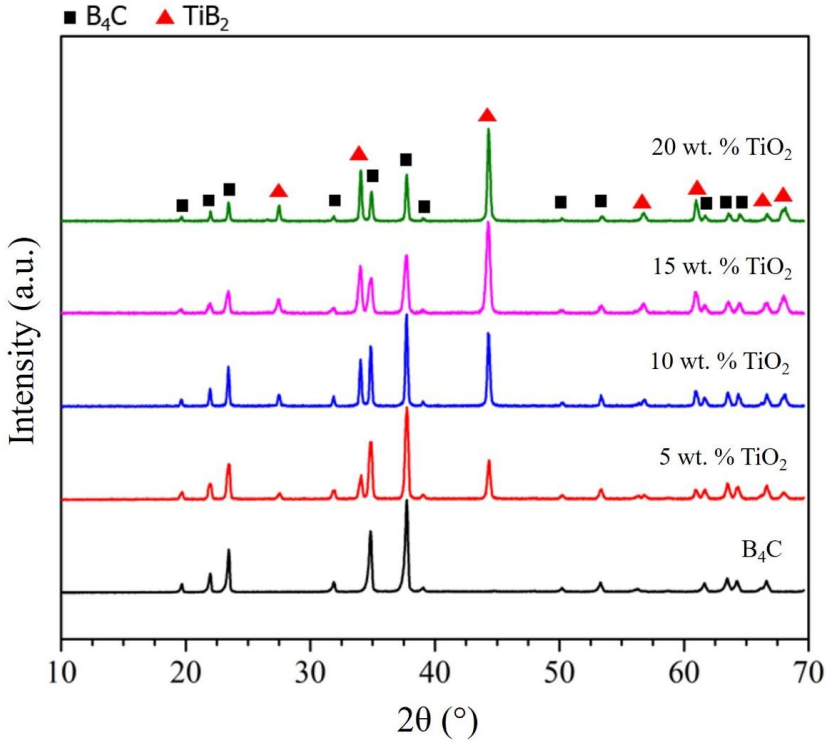


**Figure 1.** XRD spectra of the $B_4C$ matrix and $B_4Cs$ containing 5, 10, 15, 20 wt. % $TiO_2$. $B_4C$ ID:2235962, $TiB_2$ ID: 2002799 ($B_4C$ matrisi ile ağırlıkça % 5, 10, 15 ve 20 $TiO_2$ içeren $B_4C$'lerin XRD spektrası)

**Table 1.** Bulk and relative density values of the $B_4C$ matrix and $B_4Cs$ containing 5, 10, 15, 20 wt. % $TiO_2$. ($B_4C$ matrisi ile ağırlıkça % 5, 10, 15 ve 20 $TiO_2$ içeren $B_4C$'lerin yığınsal ve bağıl yoğunluk değerleri.)

| **Materials** | **Bulk Density ($gcm^{-3}$)** | **Relative Density (%)** |
|---|---|---|
| $B_4C$ | 2.490 | 98.8 |
| $B_4C$-5 wt. % $TiO_2$ | 2.516 | 97.7 |
| $B_4C$-10 wt. % $TiO_2$ | 2.537 | 96.3 |
| $B_4C$-15 wt. % $TiO_2$ | 2.589 | 96.0 |
| $B_4C$-20 wt. % $TiO_2$ | 2.619 | 94.7 |

density. The increase in bulk density can be attributed to the formation of the $TiB_2$ phase, which has a higher intrinsic density than $B_4C$. Conversely, the reduction in relative density with increasing $TiO_2$ content is likely due to porosity generated by the release of CO gas during the in-situ reaction between $TiO_2$ and $B_4C$ during sintering. These trends in relative density are consistent with the microstructural properties of the $B_4C$–$TiB_2$ composites (Fig. 2 b1–e2).

The average hardness and fracture toughness values of the $B_4C$ matrix and the in-situ $B_4C$–$TiB_2$ composites are presented in Figure 4 and Figure 5, respectively. Since the hardness of materials is generally directly proportional to their density, the measured hardness of the $B_4C$ matrix ($31.3 \pm 1.5$ GPa) aligns with expected values (~30 GPa). While no significant change was observed in the hardness of $B_4C$ with the addition of 5 wt. % $TiO_2$, its hardness decreased by approximately 11–13 % with the addition of 10, 15, and 20 wt. % $TiO_2$. This reduction is attributed to the increased porosity in the microstructure caused by higher $TiO_2$ content, which negatively impacts hardness. Furthermore, since $TiB_2$ has lower

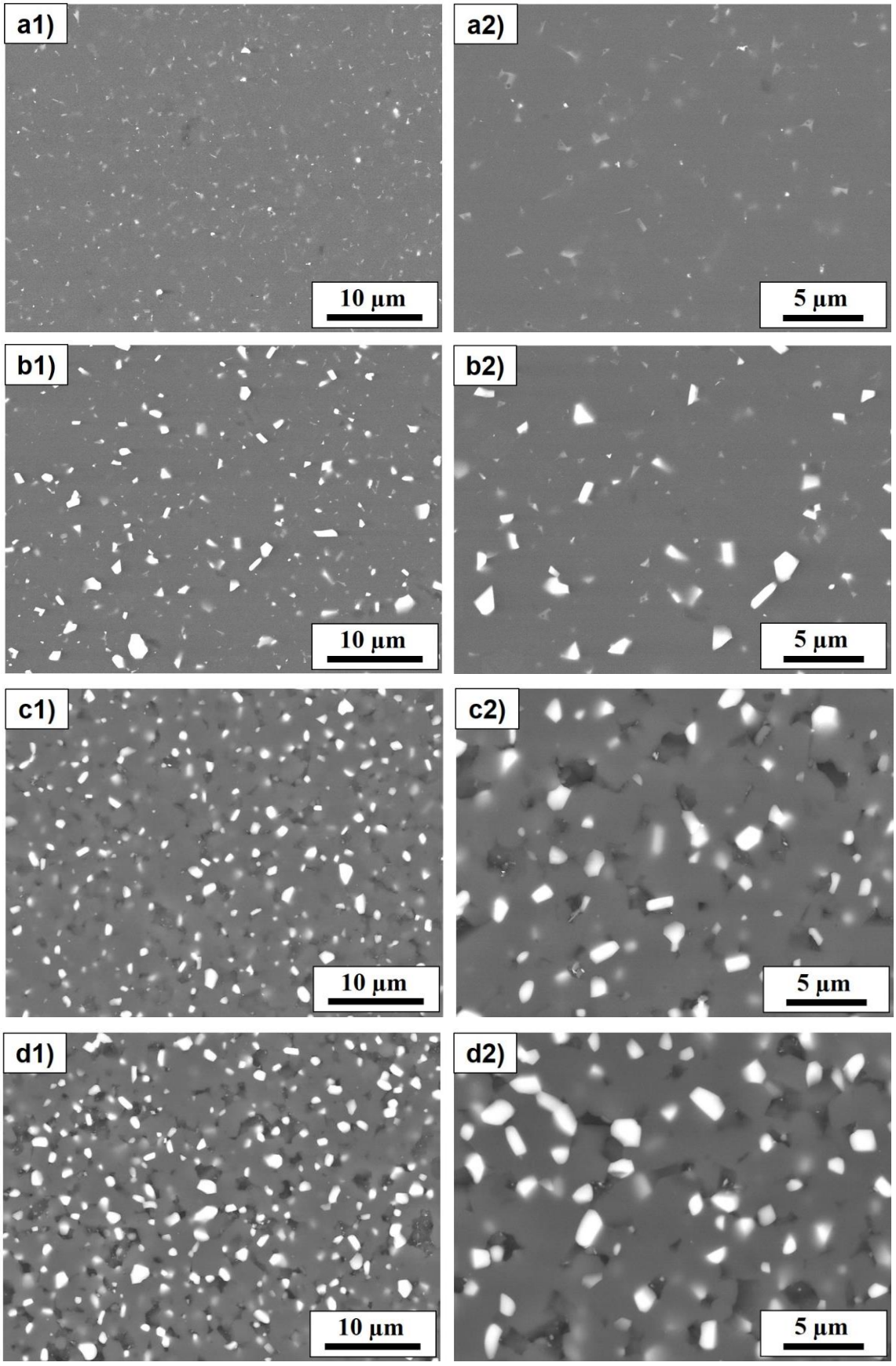
a1)
10 µm
a2)
5 µm
b1)
10 µm
b2)
5 µm
c1)
10 µm
c2)
5 µm
d1)
10 µm
d2)
5 µm

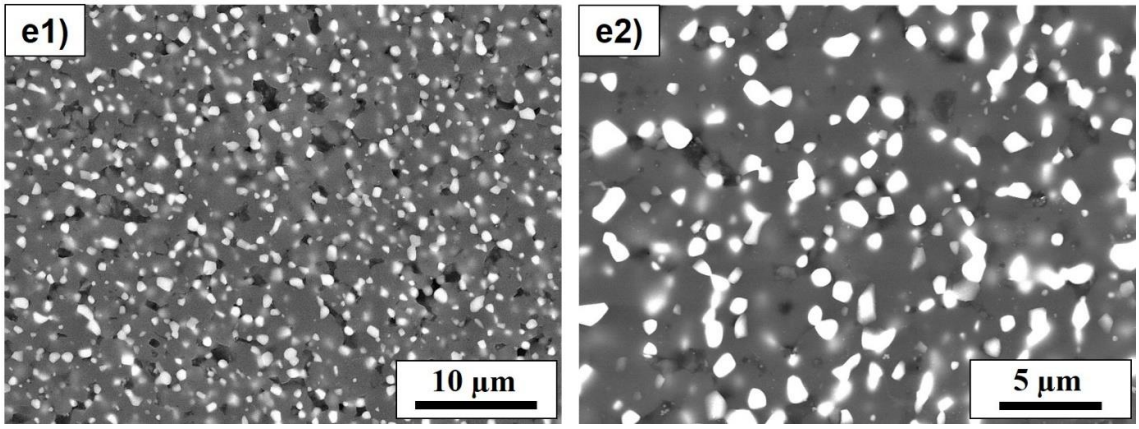


**Figure 2.** BSE-SEM images of the (a1, a2) $B_4C$ matrix and $B_4Cs$ containing (b1, b2) 5, (c1, c2) 10, (d1, d2) 15, (e1, e2) 20 wt. % $TiO_2$ at (a1, b1, c1, d1, e1) 5000X and (a2, b2, c2, d2, e2) 10000X magnifications. ((a1, a2) $B_4C$ matrisi ile (b1, b2) % 5, (c1, c2) % 10, (d1, d2) % 15 ve (e1, e2) % 20 $TiO_2$ içeren $B_4C$'lerin (a1, b1, c1, d1, e1) 5000X ve (a2, b2, c2, d2, e2) 10000X büyütmelerde BSE-SEM görüntüleri.)

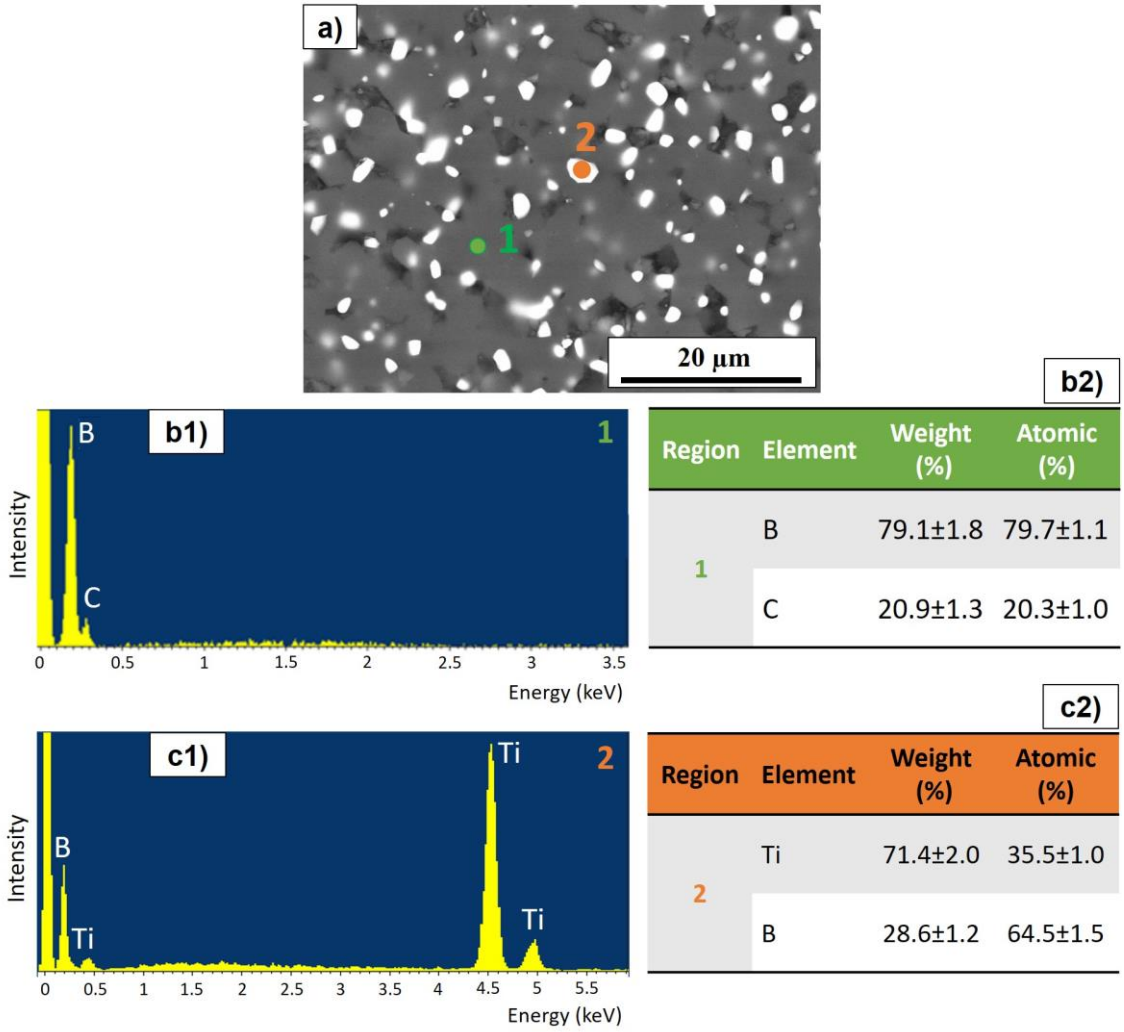


**Figure 3.** EDS-SEM analyses results of the phases present in the microstructure of $B_4C$ containing 10 wt. % $TiO_2$. (Ağırlıkça %10 $TiO_2$ içeren $B_4C$'nin mikroyapısında bulunan fazlara ait EDS-SEM analiz sonuçları.)

hardness than $B_4C$, the formation of the $TiB_2$ phase within the composite also contributed to the overall decrease in hardness of the in-situ formed $TiB_2$–$B_4C$ composites.

The fracture toughness value of the $B_4C$ matrix ($4.33\pm0.32$ MPa.m$^{1/2}$) increased by ~ 6, 43, 51 and 57 % with the addition of 5, 10, 15 and 20 wt. % $TiO_2$, respectively (Fig. 5). Additionally, Figure 6 contains representative microstructures revealing effective toughening mechanisms along the cracks created by Vickers indentation on the surfaces of the $B_4C$ matrix (a) and $B_4C$ matrix composite containing 10 wt. % $TiO_2$ (b). The $B_4C$ grain boundaries were observed to be the only factor delaying crack propagation in the $B_4C$ matrix (Fig. 6 a). On the other hand, it was determined that toughening mechanisms such as deflection, bridging and blocking provided by the $TiB_2$ phase along the crack increased the fracture toughness of $B_4C$ (Fig. 6 b). Some of the energy accumulated at the crack tip, which enables its propagation, was dissipated due to crack deflections upon encountering $TiB_2$ phases. Subsequently, the crack was thinned through crack-bridging mechanisms provided by $TiB_2$. When the crack with reduced energy encountered the $TiB_2$ phase, its propagation was halted due to blocking mechanism (Fig. 6 b).

Residual stresses arising from the large mismatch in thermal expansion coefficients between $B_4C$ ($4.5 \times 10^{-6}$ K$^{-1}$) and $TiB_2$ ($8.1 \times 10^{-6}$ K$^{-1}$) can lead to the formation of microcracks at $B_4C$–$TiB_2$ grain boundaries [25, 26]. In addition, the presence of free carbon has been reported to weaken the interfacial bonding between $B_4C$ and $TiB_2$ phases, leading to the formation of microcracks at the interfaces. These microcracks may deflect propagating cracks, thereby increasing the fracture path and energy absorption, which enhances the fracture toughness [9, 27, 28]. Moreover, the increase in fracture toughness of the $B_4C$–$TiB_2$ composite with increasing $TiB_2$ content can be attributed to the higher intrinsic fracture toughness of $TiB_2$ compared to $B_4C$.

## 4. CONCLUSION (SONUÇLAR)

In this study, $TiO_2$ was used as a sintering additive to increase the sinterability and mechanical properties of $B_4C$. $TiO_2$ powder was added to $B_4C$ matrix powder at different ratios, and the resulting compositions were sintered using the SPS technique. XRD and EDS-SEM analyses revealed that the in-situ $TiB_2$ phase was formed as a result of

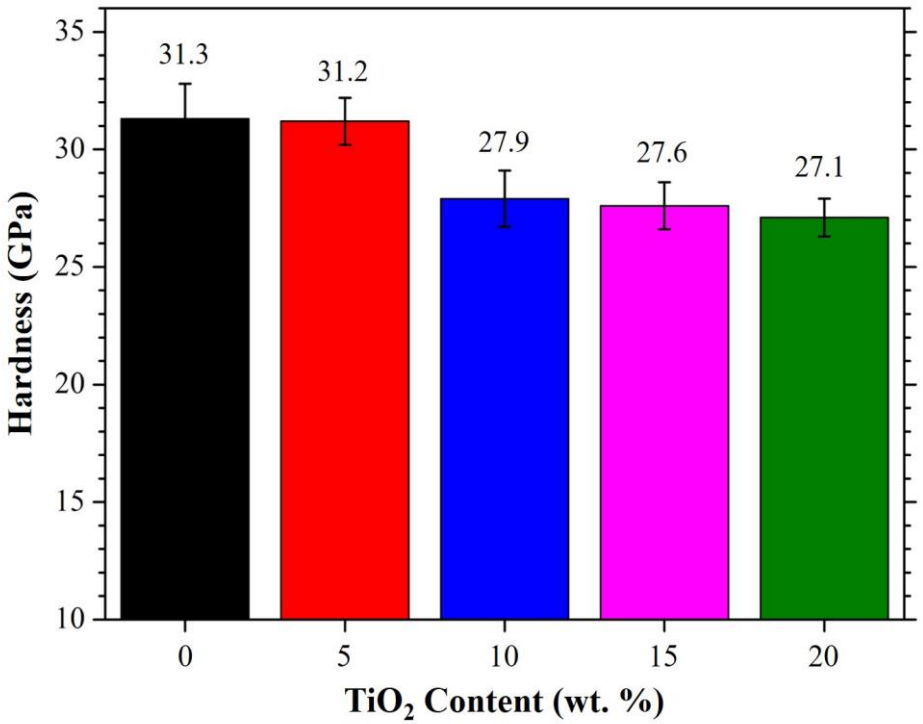


**Figure 4.** Hardness values of the $B_4C$ matrix and $B_4Cs$ containing 5, 10, 15, 20 wt. % $TiO_2$. ($B_4C$ matrisi ile ağırlıkça % 5, 10, 15 ve 20 $TiO_2$ içeren $B_4C$'lerin sertlik değerleri.)

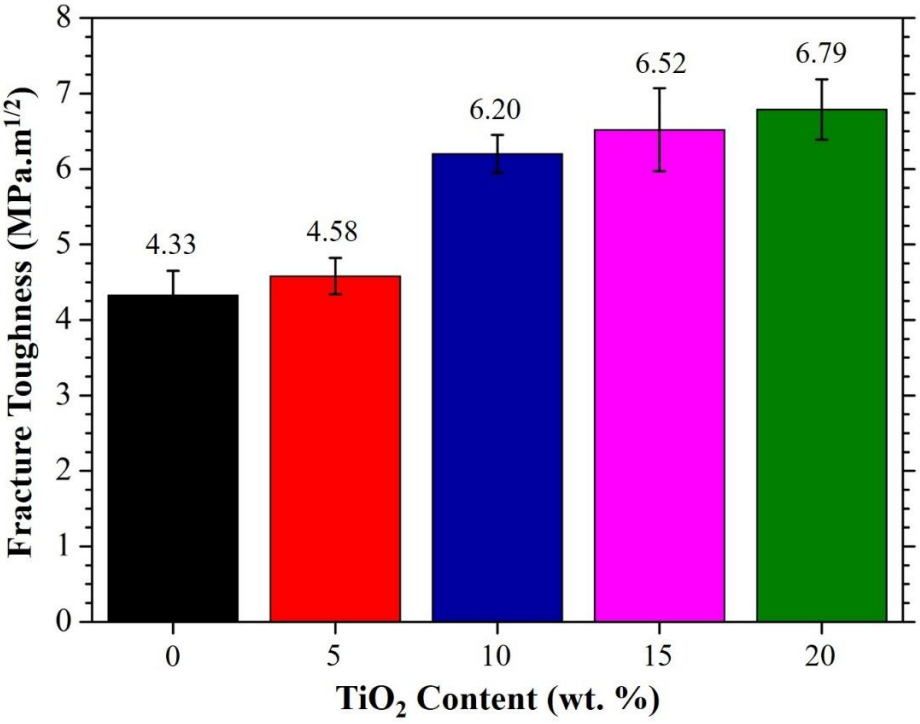


**Figure 5.** Fracture toughness values of the $B_4C$ matrix and $B_4Cs$ containing 5, 10, 15, 20 wt. % $TiO_2$. ($B_4C$ matrisi ile ağırlıkça % 5, 10, 15 ve 20 $TiO_2$ içeren $B_4C$'lerin kırılma tokluğu değerleri.)

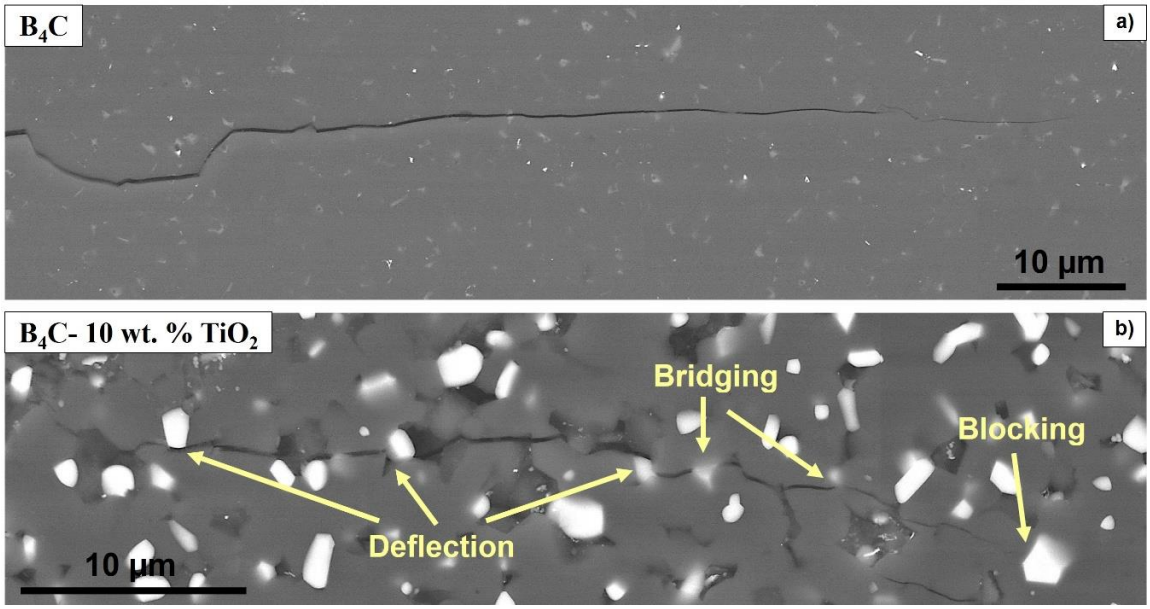


**Figure 6.** Representative BSE-SEM images of the cracks obtained by Vickers indentation on the surfaces of (a) $B_4C$ matrix and (b) $B_4C$ matrix composite containing 10 wt. % $TiO_2$. ((a) $B_4C$ matrisi ve (b) ağırlıkça % 10 $TiO_2$ içeren $B_4C$ matris kompozit yüzeylerinde Vickers indentasyon yöntemiyle elde edilen çatlaklardan alınmış temsili BSE-SEM görüntüleri.)

the reactions between $B_4C$ and $TiO_2$ during sintering. Microstructure examinations and density measurements showed that highly dense $B_4C$ matrix could be produced with the applied sintering conditions. While the density of the $B_4C$ matrix composite containing 5 wt. % $TiO_2$ was comparable to that of pure $B_4C$, increased porosity was observed in composites with 10, 15, and 20 wt. % $TiO_2$ due to CO gas evolution during the reaction. Accordingly, the relative density slightly decreased. The hardness value of the $B_4C$ matrix was obtained at the expected value (31.3±1.5 GPa). As the $TiO_2$ content increased, the hardness values tended to decrease, which corresponded proportionally to the reduction in relative density. On the other hand, the fracture toughness of the $B_4C$ matrix, determined to be approximately $4.33 \pm 0.32$ MPa.m$^{1/2}$, increased by ~ 6, 43, 51, and 57 % with the addition of 5, 10, 15, and 20 wt. % $TiO_2$, respectively. The deflection, bridging and blocking toughening mechanisms provided by the in-situ formed $TiB_2$ phase to crack propagation positively affected the fracture toughness. Additionally, the microcracks formed due to residual stress in the in-situ $B_4C$–$TiB_2$ composites contributed to an increase in the fracture toughness of $B_4C$. In applications where hardness is prioritized over fracture toughness, the addition of 5 wt. % $TiO_2$ can be considered ideal, whereas in applications that demand higher fracture toughness, increased $TiO_2$ content may be preferred.

## ACKNOWLEDGEMENTS (TEŞEKKÜR)

The Eskisehir Technical University Scientific Research Projects under the project number of 23LÖP040 and Tubitak 2209-A-Research Project Support Programme for Undergraduate Students with a number of 1919B012223499 supported this work.

## AUTHORS' CONTRIBUTIONS (YAZARLARIN KATKILARI)

***Sinem BAŞKUT:*** She took part in the execution of the experiments, analyzed the results, and carried out the writing process.

Deneylerin yürütülmesine katıldı, sonuçları analiz etti ve yazım sürecini gerçekleştirdi.

***Name YALAMA:*** She was involved in the experimental procedures.

Deneysel süreçlerin gerçekleştirilmesinde görev aldı.

***Servet TURAN:*** He contributed to the analysis of the results.

Sonuçların analiz edilmesine katkı sağladı.

## CONFLICT OF INTEREST (ÇIKAR ÇATIŞMASI)

There is no conflict of interest in this study.

Bu çalışmada herhangi bir çıkar çatışması yoktur.

## REFERENCES (KAYNAKLAR)

[1] Domnich V, Reynaud S, Haber RA, Chhowalla M. Boron carbide: structure, properties, and stability under stress. Journal of the American Ceramic Society. 94; 2011: 3605–3628.

[2] Zhu Y, Cheng H, Wang Y, An R. Effects of carbon and silicon on microstructure and mechanical properties of pressureless sintered $B_4C/TiB_2$ composites. Journal of Alloys and Compounds. 772; 2019: 537–545.

[3] Shi L, Gu Y, Chen L, Qian Y, Yang Z, Ma J. A low temperature synthesis of crystalline $B_4C$ ultrafine powders, Solid State Communication. 128; 2003: 5–7.

[4] Thevenot F. Sintering of Boron Carbide and Boron Carbide-silicon Carbide Two-phase Materials and Their Properties. Journal of Nuclear Materials. 152; 1988: 154–162.

[5] Rafi-ud-din GH et al. Ethylene Glycol Assisted Low-Temperature Synthesis of Boron Carbide Powder from Borate Citrate Precursors, Journal of Asian Ceramic Society. 2: 3; 2014: 268–274.

[6] Liu L et al. Sintering Dense Boron Carbide Without Grain Growth under High Pressure, Journal of the American Ceramic Society. 101:3; 2018:1289–1297.

[7] Tuffe S, Dubois J, Barbier G. Densification, Microstructure and Mechanical Properties of $TiB_2$-$B_4C$ Based Composites. International Journal of Refractory Metals & Hard Materials. 14; 1996: 305–310.

[8] Hwang C et al. Small Amount $TiB_2$ Addition into $B_4C$ through Sputter Deposition and Hot Pressing. Journal of the American Ceramic Society. 102: 8; 2019: 4421–4426.

[9] Khajehzadeha M, Ehsania N, Baharvandia RH, Abdollahia A, Bahaaddini M, Tamadonb A. Thermodynamical evaluation, microstructural characterization and mechanical properties of $B_4C$–$TiB_2$ nanocomposite produced by in-situ

reaction of Nano-$TiO_2$. Ceramics International. 46; 2020: 26970–26984.

[10] Zhang W, Yamashita S, Kita H. Progress in pressureless sintering of boron carbide ceramics–a review. Advanced in Applied Ceramic. 118: 4; 2019: 222-239.

[11] Sedlák R, Kovalčíková A, Múdra E, Rutkowski P, Dubiel A, Girman V, Bystrický R, Dusza J. Boron carbide/graphene platelet ceramics with improved fracture toughness and electrical conductivity. Journal of the European Ceramic Society 37: 12; 2017: 3773-3780.

[12] Mashhadi M, Nassaj ET, Sglavo VM. Pressureless sintering of boron carbide. Ceramics International. 36: 1; 2010: 151–159.

[13] Kelvin Y, Xie M, Toksoy F, Kuwelkar K, Zhang B, Krogstad JA, Haber RA, Hemker KJ. Effect of Alumina on the Structure and Mechanical Properties of Spark Plasma Sintered Boron Carbide. Journal of the American Ceramic Society 97: 11; 2014: 3710–3718.

[14] Goldstein A, Geffen Y, Goldenberg A. Boron Carbide–Zirconium Boride In Situ Composites by the Reactive Pressureless Sintering of Boron Carbide–Zirconia Mixtures. Journal of the American Ceramic Society 84: 3; 2001: 642–644.

[15] Yao W, Yan J, Li X, Chen P, Zhu Y, Zhu B. In Situ $ZrB_2$ Formation in $B_4C$ Ceramics and Its Strengthening Mechanism on Mechanical Properties. Materials. 15; 2022 7961.

[16] Perevislov SN, Lysenkov AS, Vikhman SV. Effect of Si Additions on the Microstructure and Mechanical Properties of Hot-Pressed $B_4C$. Inorganic Materials. 53: 4; 2017: 376–380.

[17] Liua G, Chenb S, Zhaoc Y, Fua Y, Wang Y. Effect of Ti and its compounds on the mechanical properties and microstructure of $B_4C$ ceramics fabricated via pressureless sintering. Ceramics International, 47: 10; 2021: 13756-13761.

[18] Şahin FÇ, Mansoor M, Cengiz M, Apak B, Yanmaz L, Balazsi K, Fogarassy Z, Derin B, Göller G, Yücel O. $B_4C$ Composites with a $TiB_2$-C Core–Shell Microstructure Produced by Self-Propagating High-Temperature Synthesis-Assisted Spark Plasma Sintering. The Journal of Physical Chemistry C. 126: 47; 2022: 20114-20126.

[19] Twardowska A, Kowalski M. The Microstructure, Mechanical, and Friction-Wear Properties of Boron Carbide-Based Composites with $TiB_2$ and SiC Formed In Situ by Reactive Spark Plasma Sintering. Materials, 17; 2024: 2379.

[20] Wang S, Yuan Y, Hanc W, Yin Z. Microstructure and mechanical properties of $B_4C$-$TiB_2$ composite ceramic fabricated by reactive spark plasma sintering. International Journal of Refractory Metals and Hard Materials. 92; 2020: 105307.

[21] Rangel ER. Fracture Toughness Determinations by Means of Indentation Fracture, Nanocomposites with Unique Properties and Applications in Medicine and Industry. InTechOpen. 2011: ISBN:978-953-307-351-4.

[22] Kakazey M, Vlasova M, Gonzalez-Rodriguez JG, Dominguez-Patino M, Leder R. X-ray and EPR study of reactions between $B_4C$ and $TiO_2$, Materials Science Engineering A. 418; 2006: 111-114.

[23] Levin L, Frage N, Dariel MP. The effect of Ti and $TiO_2$ additions on the pressureless sintering of $B_4C$. Metallurgical and Materials Transactions A, 30;1999: 3201-3210.

[24] Yang LK, Shen P, Guo R-F, Jiang Q-C. The role of $TiO_2$ incorporation in the preparation of $B_4C$/Al laminated composites with high strength and Toughness. Ceramics International. 44:13; 2018: 15219-15227.

[25] Asghar Z, Aziz T, Khan AR, Shah A, Waqas H, Ali F, Rasul HT, Khan MF. High-Hardness High-Fracture-Toughness $B_4C$-$TiB_2$ Composite Produced by Reactive Hot Pressing. Journal of Materials Engineering and Performance. 32; 2023: 7225–7233.

[26] He Q et al. Microstructures and Mechanical Properties of $B_4C$-$TiB_2$-SiC Composites Fabricated by Ball Milling and Hot Pressing. Journal of the Eıropean Ceramic Society. 38:7; 2018: 2832–2840.

[27] Sigl LS, Kleebe HJ. Microcracking in $B_4C$-$TiB_2$ Composites. Journal of American Ceramic Society. 78: 9; 1995: 2374–2380.

[28] Wang W, Lian J, Ru H. Pressureless sintered SiC matrix toughened by in situ synthesized

$TiB_2$: process conditions and fracture Toughness. Ceramics International. 38; 2012: 2079-2085.